ELECTRONIC SUPPORTING INFORMATION

Increasing the nuclearity and spin ground state in a new family of ferromagnetically-coupled {Ni_{10}} disk-like complexes bearing exclusively end-on bridging azido ligands

Jasmin Krause,[a] Dimitris I. Alexandropoulos,[b] Luca M. Carrella,[a] Eva Rentschler*[a] and Theocharis C. Stamatatos*[a,b]

---

[a] Institute of Inorganic and Analytical Chemistry, Johannes Gutenberg University Mainz, Duesbergweg 10-14, D-55128 Mainz, Germany

[b] Department of Chemistry, 1812 Sir Isaac Brock Way, Brock University, L2S 3A1 St. Catharines, Ontario, Canada

Corresponding authors: rentschler@uni-mainz.de (E. Rentschler); tstamatatos@brocku.ca (Th. C. Stamatatos)

Experimental Section

Synthesis. All manipulations were performed under aerobic conditions using materials (reagent grade) and solvents as received, unless otherwise noted. Green crystals of the $[Ni_2(H_2O)(piv)_4(pivH)_4]$ (pivH = pivalic acid) precursor were obtained in 70-80% yield by following a previously described synthetic route.[S1] The green microcrystalline solid $Ni(O_2CPh)_2$ was prepared in the same manner as the $Mn(O_2CPh)_2$ analogue, described elsewhere.[S2] For the high-yield and high-purity synthesis of the reported compounds **1**-**4**, the dehydration of all the lanthanide nitrate starting materials was found to be imperative. Therefore, the $Ln(NO_3)_3{\cdot}6H_2O$ salts were first dried under ultra-high vacuum for 24 h and the resulting solids were then heated at 150°C for 8 h to yield the anhydrous $Ln(NO_3)_3$ precursors.

Caution! Azide salts, and their corresponding metal complexes, are potentially explosive; such compounds should be synthesized and used in small quantities and treated with utmost care at all times. None of the reported compounds detonate on shock or spark under the reported conditions. Thus, complexes **1**-**4** were found to be safe when used in small quantities. However, the potentially explosive nature of **1**-**4**, due to the presence of a large number of azido groups, renders the use of thermogravimetric and other high-temperature techniques impossible. The vacuum dryness of all complexes was also avoided for safety reasons as well as due to the immediate loss of their crystallinity, most likely due to the partial or complete loss of the coordinated and lattice MeCN molecules. These solvation/de-solvation effects were also observed in the family of $[M^{II}_7(N_3)_{12}(MeCN)_{12}](ClO_4)_2$ SMM complexes recently reported by few of us (see refs. 12 and 13 of the main text).

$[Ni_{10}(N_3)_{18}(MeCN)_{14}][Gd(NO_3)_5]$ (1): To a stirred, pale green solution of $[Ni_2(H_2O)(piv)_4(pivH)_4]$ (0.19 g, 0.20 mmol) and $Gd(NO_3)_3$ (0.04 g, 0.10 mmol) in MeCN (10 mL) was added dropwise Me_3SiN_3 (0.35 mL, 2.60 mmol). The resulting deep green solution was stirred for 5 min, filtered, and the filtrate was diffused with Et_2O (20 mL). Green rod-like crystals of **1**$\cdot$6MeCN$\cdot$2H_2O were obtained after 3-4 days in ~65% yield (based on the total available Ni). CCDC deposition number: 1864765.

$[Ni_{10}(N_3)_{18}(MeCN)_{14}][Tb(NO_3)_5]$ (2): This complex was prepared in the exact same manner as complex **1** but using $Tb(NO_3)_3$ (0.04 g, 0.10 mmol) in place of $Gd(NO_3)_3 \cdot 6H_2O$. Green rod-like crystals of **2**·4MeCN·$2H_2O$ were obtained after 3-4 days in ~70% yield (based on the total available Ni). CCDC deposition number: 1864766.

$[Ni_{10}(N_3)_{18}(MeCN)_{14}][Dy(NO_3)_5]$ (3): To a stirred, pale green solution of $Ni(O_2CPh)_2$ (0.06 g, 0.20 mmol) and $Dy(NO_3)_3$ (0.04 g, 0.10 mmol) in MeCN (10 mL) was added dropwise Me_3SiN_3 (0.35 mL, 2.60 mmol). The resulting deep green solution was stirred for 5 min, filtered, and the filtrate was diffused with Et_2O (20 mL). Green rod-like crystals of **3**·4MeCN·H_2O were obtained after 3-4 days in ~60% yield (based on the total available Ni). CCDC deposition number: 1864767.

$[Ni_{10}(N_3)_{18}(MeCN)_{14}][Y(NO_3)_5]$ (4): This complex was prepared in the exact same manner as complex **1** but using $Y(NO_3)_3$ (0.03 g, 0.10 mmol) in place of $Gd(NO_3)_3 \cdot 6H_2O$. Green rod-like crystals of **4**·4MeCN were obtained after 3-4 days in ~70% yield (based on the total available Ni). CCDC deposition number: 1869182.

IR Spectroscopy. Selected IR data for **1** (KBr): *v*= 3000 (w), 2938 (w), 2315 (w), 2288 (w), 2252 (w), 2109 (vs), 2069 (vs), 1482 (s), 1372 (m), 1301 (s), 1229 (s), 1027 (m), 938 (w), 918 (w), 816 (w), 741 (m), 686 (w), 644 (m), 627 (m), 591 (w). Selected IR data for **2** (KBr): *v*= 2996 (w), 2937 (w), 2358 (w), 2317 (w), 2289 (w), 2095 (vs), 2066 (vs), 1484 (s), 1370 (w), 1302 (s), 1229 (m), 1026 (m), 939 (w), 815 (w), 742 (m), 644 (m), 627 (m). Selected IR data for **3** (KBr): *v*= 2981 (w), 2937 (w), 2314 (w), 2287 (w), 2107 (vs), 2065 (vs), 1624 (m), 1570 (w), 1481 (m), 1404 (s), 1369 (m), 1299 (s), 1227 (s), 1070 (w), 1027 (m), 939 (w), 815 (w), 721 (m), 683 (m), 670 (m), 643 (m), 626 (m), 591 (w). Selected IR data for **4** (KBr): *v*= 3001(w), 2938 (w), 2315 (w), 2288 (w), 2252 (w), 2094 (vs), 2065 (vs), 1486 (s), 1371 (m), 1304 (s), 1229 (m), 1028 (m), 939 (w), 816 (w), 745 (m), 645 (m), 627 (m).

The IR spectra of all complexes **1**-**4** are shown in Fig. S1 as a single superimposed image to confirm: (i) their isostructurality in the solid-state, (ii) the presence of end-on

bridging N_3^- groups (IR bands in the region ~2065-2100 cm^{-1}),[S3] and (iii) the presence of bidentate chelating NO_3^- groups (IR bands of ~1480, ~1300 and ~1030 cm^{-1}; $\Delta\nu = \nu_1 - \nu_4$ = ~180 cm^{-1}; $\Delta\nu$ increases as the coordination of the nitrate group increases for monodentate to bidentate and/or bridging; The size of this splitting is indicative of a strong interaction of the oxygens of the nitrate with the 4*f*-metal ion and typical of bidentate binding).[S4,S5] Furthermore, in Fig. S2 we show the changes of the IR spectra of representative complex **3** with time, which confirm the degradation of the dried solid-state samples upon exposure to air for a prolonged time. The solvation/de-solvation effects within **3** are evidenced by the disappearance of the IR bands attributed to the coordinated/lattice MeCN molecules of the wet-sample (2250-2350 and 2900-3000 cm^{-1}), and their replacement by the broad IR band ~3400 cm^{-1}, assignable to H_2O molecules, for two different air dried-samples of **3** (dryness for 2 h and 24 h, respectively).[S5]

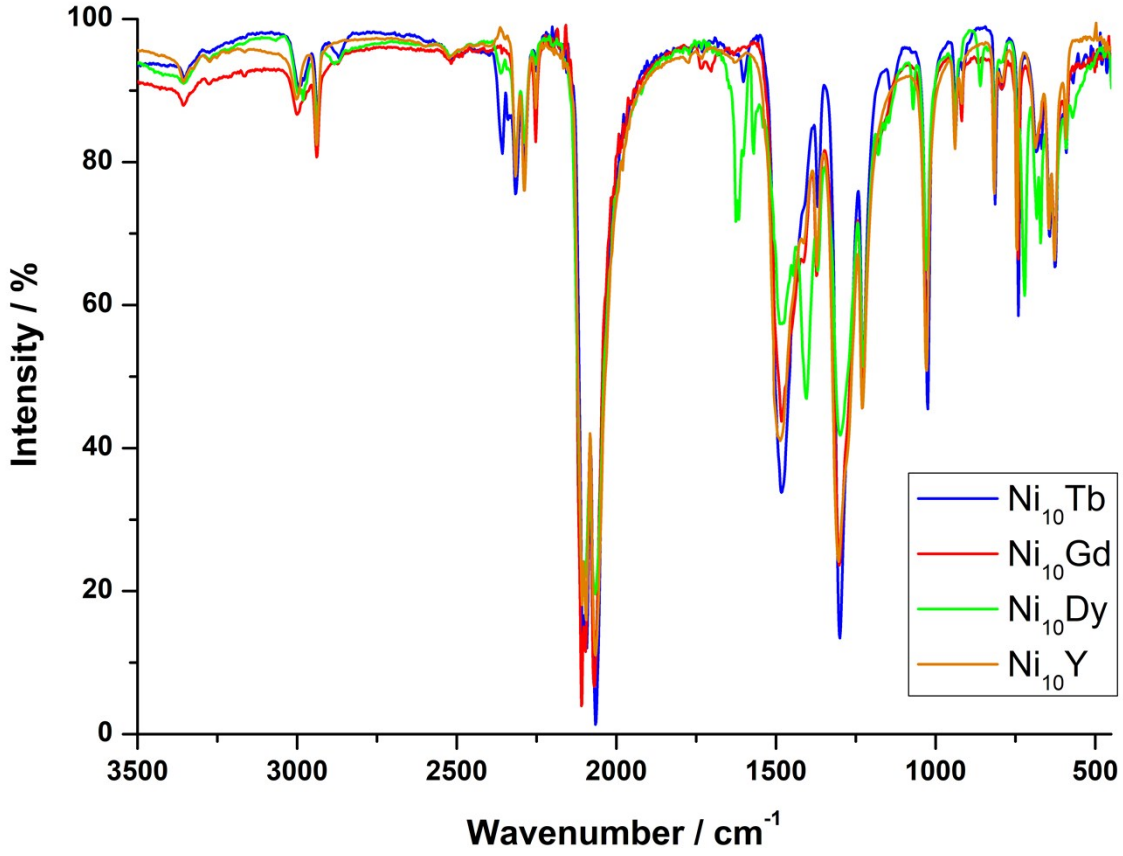

Fig. S1 IR spectra of complexes **1**-**4**.

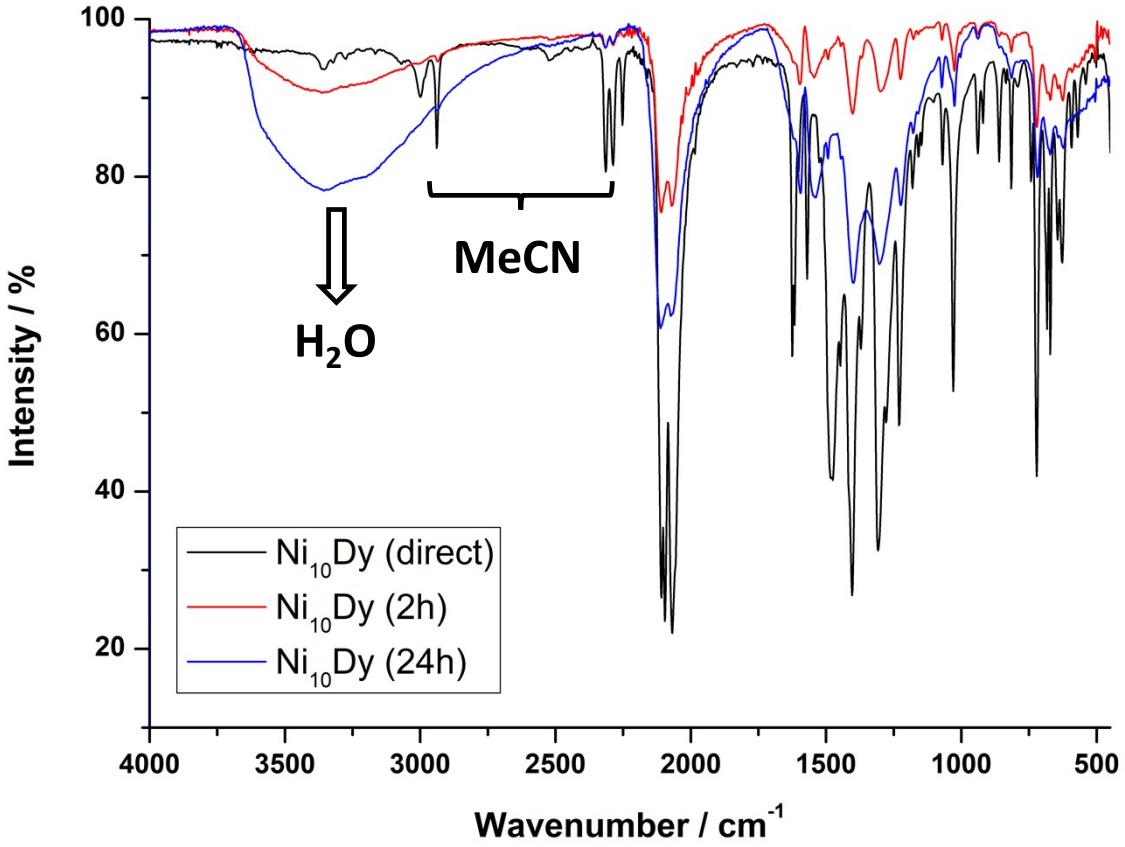

Fig. S2 IR spectra of representative complex **3** as a function of time. The exchange of coordinated/lattice MeCN by H_2O molecules is evidenced by the disappearance of the IR bands in the 2250-2350 and 2900-3000 cm^{-1} regions of the wet-sample and the emergence of a broad band ~3400 cm^{-1} for the two dried-samples, respectively.

Single-crystal X-ray Crystallography. X-ray diffraction data for the structure analysis were collected from suitable single-crystals on a Bruker SMART with an APEX II CCD detector (for **1**, **2** and **3**) and on an Oxford diffraction Xcalibur with a Sapphire3 CCD detector (for **4**) equipped with an Oxford cooling system operating at 173(2) K. Graphite-monochromated Mo-Kα radiation (λ = 0.71073 Å; for **1**, **2**, **3**) and Cu-Kα radiation (λ = 1.54184 Å; for **4**) from fine focus sealed X-ray tube was used throughout. Data reduction and absorption correction were done with *Bruker Apex* v3.0[S6] and *SADABS*[S7] (for **1**, **2** and **3**) or with *Rigaku CrysAlisPro*[S8] (for **4**), respectively. Structures were solved with *SHELXT*[S9] and refined by full-matrix least-squares on F^2 using *SHELXL*[S10], interfaced through *OLEX2*[S11]. All non-hydrogen atoms were refined with anisotropic displacement

parameters, while all hydrogen atoms have been placed on idealized positions using a riding model. Two independent $[Ni_{10}(N_3)_{18}(MeCN)_{14}]^{2+}$ cationic species are present in **1**, while only half of each cation is part of the asymmetric unit. One cation is disordered over two positions with a free refined ratio of 0.86 to 0.14. Due to the large difference in ratio only the nickel(II) ions were refined over two positions, while the azides and the acetonitrile molecules were only refined on the main positions. For the $[Gd(NO_3)_5]^{2-}$ anion and the second $[Ni_{10}(N_3)_{18}(MeCN)_{14}]^{2+}$ cation no disorder was found. The asymmetric unit of **4**, consists of half of the $[Ni_{10}(N_3)_{18}(MeCN)_{14}]^{2+}$ cation and half of the $[Y(NO_3)_5]^{2-}$ anionic species. The $[Y(NO_3)_5]^{2-}$ anion is disordered via the inversion center over two positions with a ratio of 0.5 to 0.5. The poor quality of the crystals of complex **1** is attributed to the immediate loss of lattice crystallization solvents and subsequently the fast degradation and loss of crystallinity. This resulted in a very weak diffraction of all selected crystals and consequently a rather poor X-ray diffraction data set.

Table S1. Crystallographic Data for Complexes **1**-**4**

Complex	**1**·6MeCN·2H_2O	**2**·4MeCN·2H_2O	**3**·4MeCN·H_2O	**4**·4MeCN
Formula	$C_{40}H_{60}N_{79}Ni_{10}GdO_{17}$	$C_{36}H_{54}N_{77}Ni_{10}TbO_{17}$	$C_{35}H_{52.5}N_{77}Ni_{10}DyO_{16}$	$C_{36}H_{54}N_{77}Ni_{10}YO_{15}$
FW / g mol^{-1}	2664.02	2583.58	2557.64	2481.57
Crystal system	Triclinic	Triclinic	Triclinic	Triclinic
Space group	P-1	P-1	P-1	P-1
a / Å	11.156(2)	11.160(2)	11.165(2)	11.0684(12)
b / Å	17.898(3)	19.509(4)	19.456(4)	14.2915(16)
c / Å	28.868(4)	23.698(4)	23.633(5)	16.0071(14)
α / °	105.722(4)	106.432(4)	106.086(6)	78.715(9)
β / °	93.827(4)	91.339(4)	91.383(6)	84.321(8)
γ / °	103.427(4)	94.085(4)	93.738(6)	81.693(9)
V / $Å^3$	5344.8(13)	4931.1(16)	4917.6(16)	2450.5(4)
Z	2	2	2	1
T / K	173(2)	173(2)	173(2)	173(2)
λ / Å	0.71073	0.71073	0.71073	1.54184
Radiation type	Mo Ka	Mo Ka	Mo Ka	Cu Ka
ρ_{calc} / g cm^{-3}	1.655	1.740	1.727	1.682
μ / mm^{-1}	2.417	2.661	2.707	3.552
Measd /	47462 / 20931	60571 / 19380	39524 / 18320	16670 / 7748

independent (R_{int}) reflns	(0.1057)	(0.0953)	(0.2470)	(0.0572)
Obsd reflns [$I > 2\sigma(I)$]	10919	10656	4257	3621
R_1[a]	0.1433	0.0652	0.0882	0.0537
wR_2[b]	0.2949	0.1353	0.1777	0.1177
GOF on F^2	1.064	1.016	0.847	0.849
$(\Delta\rho)_{max,min}$ / e Å^{-3}	2.359, -2.081	1.755, -1.352	1.596, -1.151	0.749, -0.363

[a] $R_1 = \Sigma(||F_o| - |F_c||)/\Sigma|F_o|$. [b] $wR_2 = [\Sigma[w(F_o^2 - F_c^2)^2]/\Sigma[w(F_o^2)^2]]^{1/2}$, $w = 1/[\sigma^2(F_o^2) + [(ap)^2 + bp]$, where $p = [\max(F_o^2, 0) + 2F_c^2]/3$.

Table S2. Selected Interatomic Distances (Å) and Angles (°) for Complex **3**

Bond lengths			
Ni1-N1	2.088(14)	Ni6-N13	2.116(17)
Ni1-N4	2.105(17)	Ni6-N16	2.164(15)
Ni1-N7	2.114(16)	Ni6-N37	2.018(16)
Ni1-N10	2.064(17)	Ni6-N40	2.084(16)
Ni1-N13	2.101(16)	Ni6-N60	2.090(18)
Ni1-N16	2.107(16)	Ni6-N61	2.08(2)
Ni2-N1	2.091(15)	Ni7-N4	2.149(17)
Ni2-N4	2.140(17)	Ni7-N16	2.097(16)
Ni2-N19	2.128(16)	Ni7-N22	2.106(17)
Ni2-N22	2.112(17)	Ni7-N40	2.093(16)
Ni2-N25	2.140(17)	Ni7-N43	2.067(17)
Ni2-N28	2.085(16)	Ni7-N62	2.074(16)
Ni3-N1	2.162(15)	Ni8-N22	2.110(17)
Ni3-N7	2.176(16)	Ni8-N25	2.183(16)
Ni3-N19	2.162(18)	Ni8-N43	2.083(17)
Ni3-N31	2.012(19)	Ni8-N46	2.035(19)
Ni3-N52	2.052(17)	Ni8-N63	2.026(14)
Ni3-N55	2.034(17)	Ni8-N64	2.05(2)
Ni4-N7	2.189(16)	Ni9-N25	2.177(17)
Ni4-N10	2.146(17)	Ni9-N28	2.120(16)
Ni4-N31	2.026(18)	Ni9-N46	2.08(2)
Ni4-N34	2.086(17)	Ni9-N49	2.069(16)
Ni4-N56	2.099(18)	Ni9-N65	2.09(2)
Ni4-N57	2.095(19)	Ni9-N66	2.089(14)
Ni5-N10	2.094(16)	Ni10-N19	2.185(15)
Ni5-N13	2.181(16)	Ni10-N28	2.127(16)
Ni5-N34	2.040(18)	Ni10-N49	2.141(17)
Ni5-N37	2.090(17)	Ni10-N52	2.020(18)
Ni5-N58	2.08(2)	Ni10-N67	2.071(17)

Ni5-N59	2.085(17)	Ni10-N68	2.03(2)
Dy1-O1	2.391(19)	Dy1-O8	2.41(2)
Dy1-O2	2.358(17)	Dy1-O10	2.404(19)
Dy1-O4	2.428(19)	Dy1-O11	2.478(17)
Dy1-O5	2.380(15)	Dy1-O13	2.448(16)
Dy1-O7	2.55(2)	Dy1-O14	2.434(17)

Bond angles			
Ni1-N1-Ni2	100.1(6)	Ni3-N7-Ni4	94.9(6)
Ni1-N1-Ni3	98.7(6)	Ni3-N19-Ni10	94.3(6)
Ni1-N4-Ni2	98.0(7)	Ni3-N31-Ni4	105.6(8)
Ni1-N4-Ni7	98.0(8)	Ni5-N10-Ni4	98.7(6)
Ni1-N7-Ni3	97.5(6)	Ni5-N34-Ni4	102.5(8)
Ni1-N7-Ni4	96.3(7)	Ni6-N13-Ni5	97.2(7)
Ni1-N10-Ni4	99.2(7)	Ni6-N37-Ni5	103.4(8)
Ni1-N10-Ni5	100.7(7)	Ni6-N40-Ni7	98.9(7)
Ni1-N13-Ni5	96.7(7)	Ni7-N16-Ni1	99.6(7)
Ni1-N13-Ni6	99.4(7)	Ni7-N16-Ni6	96.3(6)
Ni1-N16-Ni6	97.7(6)	Ni7-N22-Ni2	99.5(7)
Ni2-N1-Ni3	98.2(7)	Ni7-N22-Ni8	98.1(7)
Ni2-N4-Ni7	97.2(6)	Ni7-N43-Ni8	100.2(8)
Ni2-N19-Ni3	97.1(7)	Ni8-N22-Ni2	98.4(8)
Ni2-N19-Ni10	96.1(6)	Ni8-N46-Ni9	103.6(8)
Ni2-N25-Ni8	95.3(7)	Ni9-N25-Ni8	95.6(6)
Ni2-N25-Ni9	96.0(7)	Ni9-N28-Ni10	98.5(7)
Ni2-N28-Ni9	99.4(7)	Ni9-N49-Ni10	99.6(7)
Ni2-N28-Ni10	99.2(6)	Ni10-N52-Ni3	103.0(8)

Table S3. Continuous Shape Measures of the 10-Coordinate Lanthanide Coordination Polyhedra in Complexes **1**-**4**.[a]

Polyhedron[b]	Gd1	Tb1	Dy1	Y1
DP-10	36.584	35.790	35.272	34.454
EPY-10	25.535	25.815	25.564	24.668
OBPY-10	15.779	16.410	17.198	15.542
PPR-10	10.922	11.479	11.139	12.073
PAPR-10	11.274	9.747	9.850	10.985
JBCCU-10	10.391	8.463	7.854	8.608

JBCSAPR-10	5.601	5.478	5.192	4.880
JMBIC-10	6.643	6.144	5.934	6.549
JATDI-10	18.122	19.321	18.590	17.797
JSPC-10	3.270	4.064	3.859	4.361
SDD-10	2.933	2.907	2.819	4.028
TD-10	**2.246**	**2.038**	**2.003**	**3.178**
HD-10	7.225	5.292	5.002	5.536

[a] The values in boldface indicate the closest polyhedron according to the Continuous Shape Measures (CShM). [b] Abbreviations: DP-10, Decagon; EPY-10, Enneagonal pyramid; OBPY-10, Octagonal bipyramid; PPR-10, Pentagonal prism; PAPR-10, Pentagonal antiprism; JBCCU-10, Bicapped cube J15; JBCSAPR-10, Bicapped square antiprism J17; JMBIC-10, Metabidiminished icosahedron J62; JATDI-10, Augmented tridiminished icosahedron J64; JSPC-10, Sphenocorona J87; SDD-10, Staggered Dodecahedron; **TD-10, Tetradecahedron**; HD-10 Hexadecahedron.

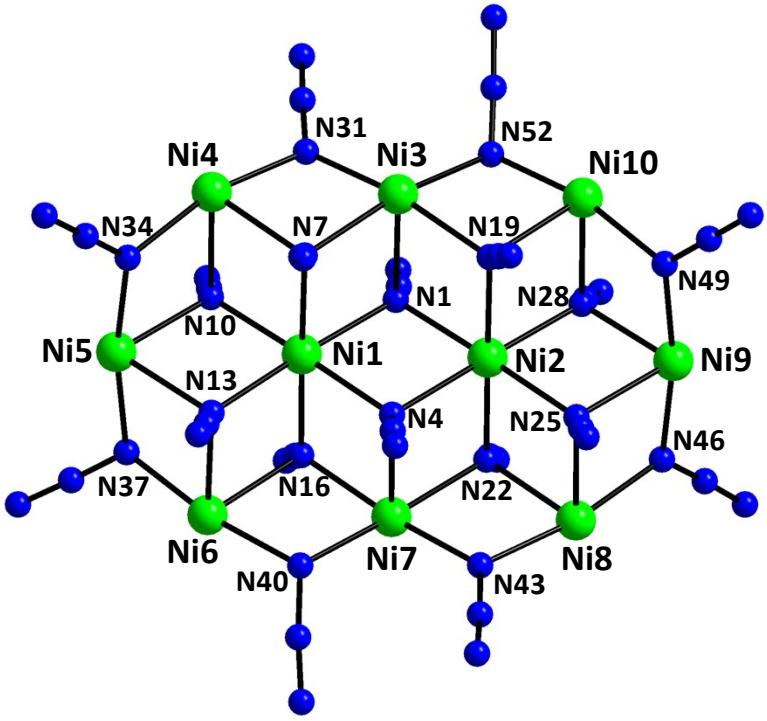

Fig. S3 The $[Ni_{10}(\mu_3\text{-}N_3)_{10}(\mu\text{-}N_3)_8]^{2+}$ inorganic core of **3**. Color scheme: Ni^{II} green, N blue.

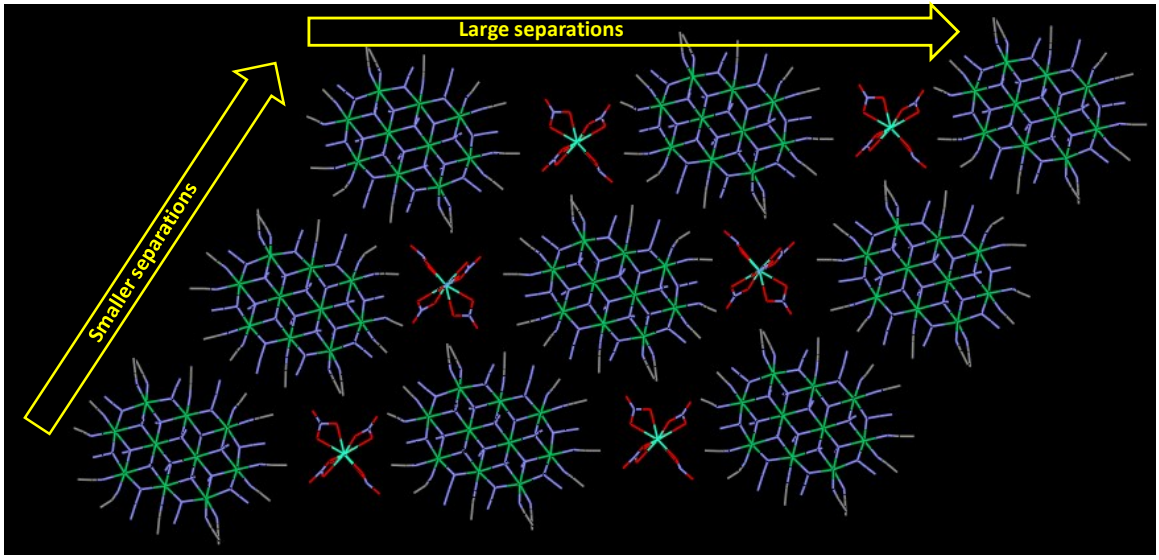

Fig. S4 The packing of the $[Ni_{10}(N_3)_{18}(MeCN)_{14}][Dy(NO_3)_5]$ clusters in the crystal of **3**, highlighting the orientations of the $[Dy(NO_3)_5]^{2-}$ counterions and their effect on the intermolecular separations between the $\{Ni_{10}\}^{2+}$ cations. The shortest Ni···Ni and Ln···Ln intermolecular separations for complexes **1**, **2** and **4** are: 8.6 and 15.7 Å (for **1**), 8.5 and 14.8 Å (for **2**) and 9.8 and 17.6 Å (for **4**), respectively.

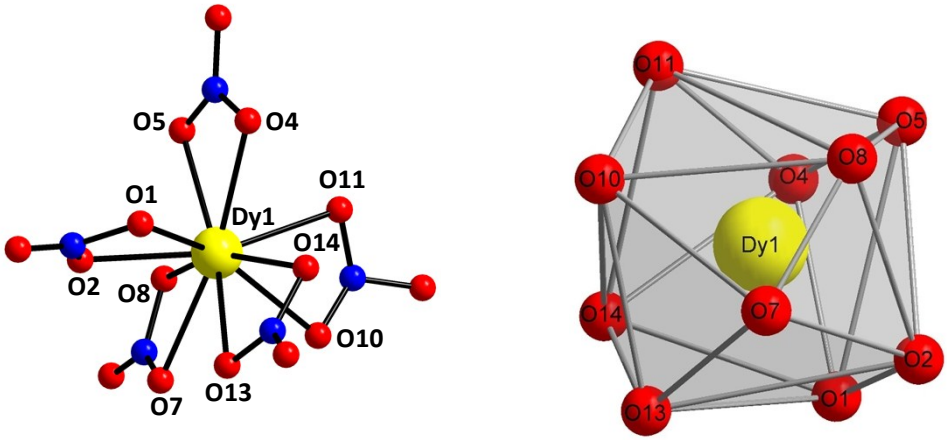

Fig. S5 Labeled structure of the $[Dy(NO_3)_5]^{2-}$ counterion in **3** (left), and the tetradecahedral geometry of the Dy^{III} atom (right). Points connected by the grey lines define the vertices of the ideal polyhedron. Color scheme: Dy^{III} yellow, N blue, O red.

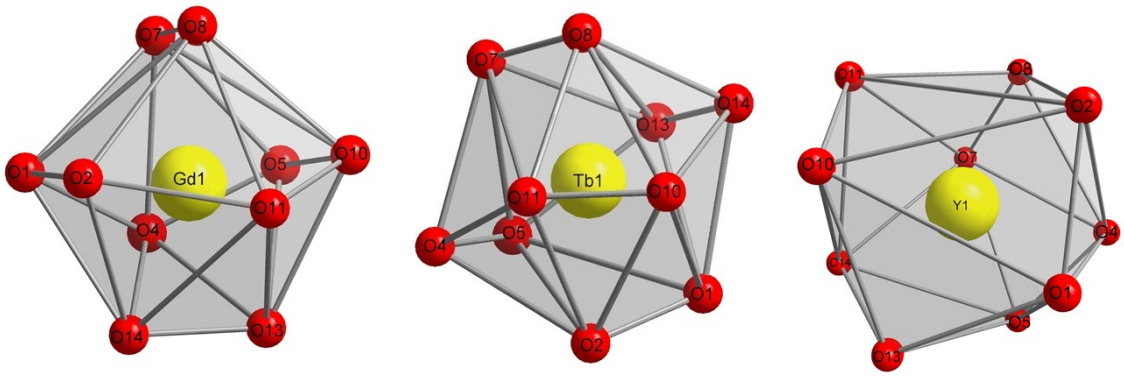

Fig. S6 Tetradecahedral coordination geometries of Gd1, Tb1 and Y1 atoms in the structures of **1**, **2**, and **4**, respectively. Points connected by the grey lines define the vertices of the ideal polyhedron. The so-called Continuous Shape Measures (CShM) approach essentially allows one to numerically evaluate by how much a particular structure deviates from an ideal shape. The obtained CShM values are listed in Table S3. Values of CShM between 0.1 and 3 usually correspond to a not negligible but still small distortion from ideal geometry, while values larger than 3 refer to very distorted coordination environments.

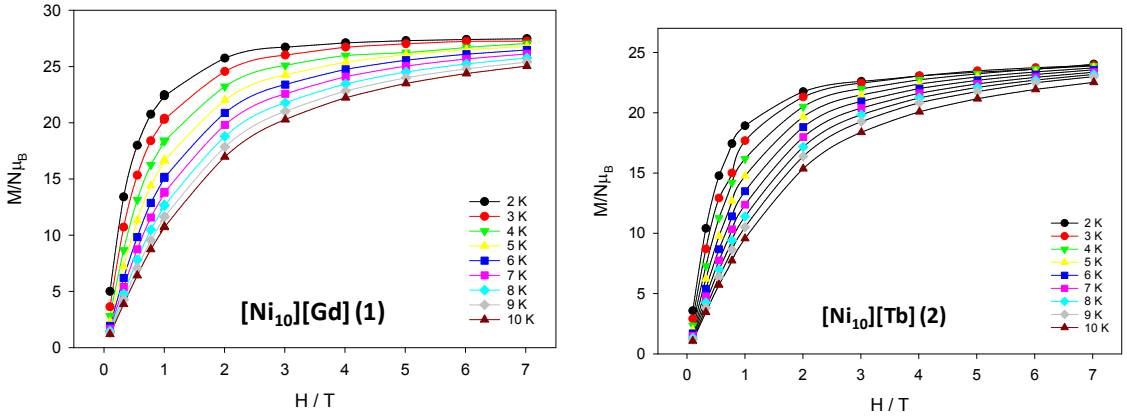

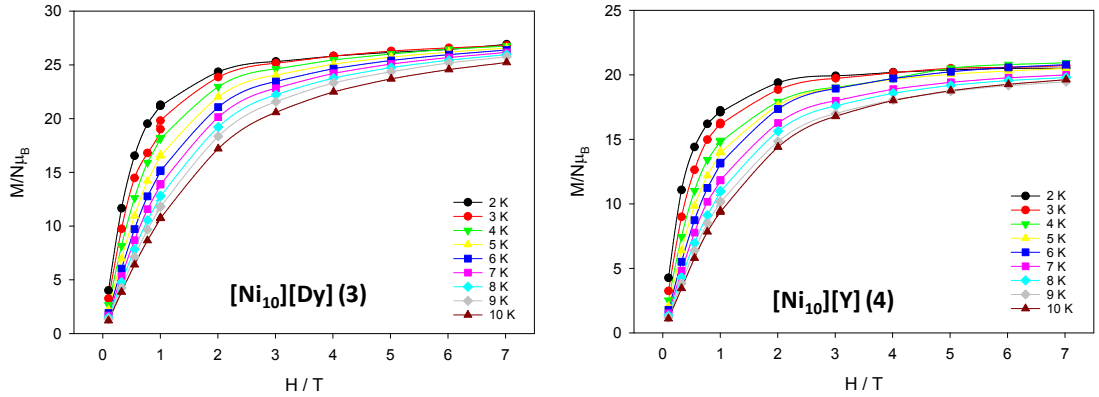

Fig. S7 Magnetization (*M*) *vs.* field (*H*) plots for complexes **1**-**4** at various low temperatures; the solid lines are only guides for the eye.

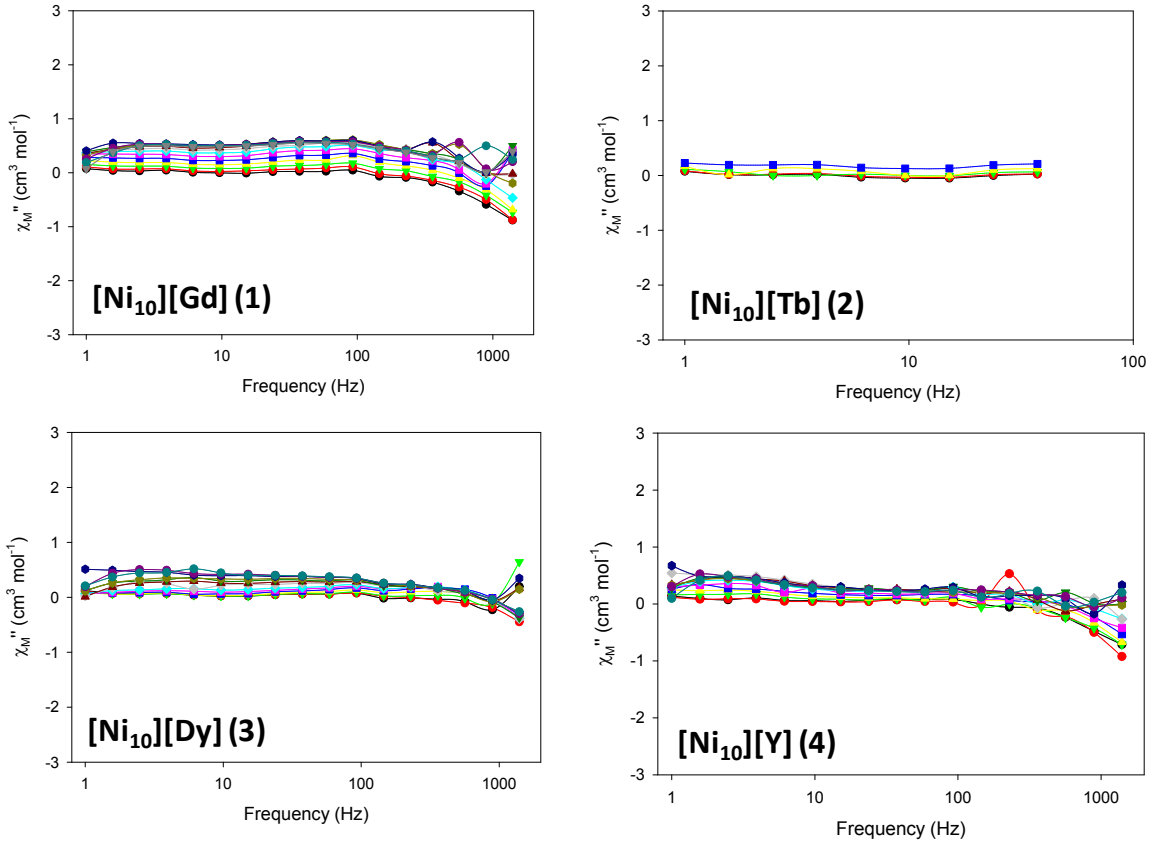

Fig. S8 Out-of-phase (χ_M'') *ac* magnetic susceptibility signals for **1**-**4** as a function of *ac* frequency at 2 K and various *dc* fields (from 0 to 3000 Oe); the solid lines are only guides for the eye.

References

[S1] G. Chaboussant, R. Basler, H.- U. Güdel, S. Ochsenbein, A. Parkin, S. Parsons, G. Rajaraman, A. Sieber, A. A. Smith, G. A. Timco and R. E. P. Winpenny, *Dalton Trans.*, 2004, 2758.

[S2] M. W. Wemple, H. -L. Tsai, S. Wang, J. P. Claude, W. E. Streib, J. C. Huffman, D. N. Hendrickson and G. Christou, *Inorg. Chem.*, 1996, **35**, 6437.

[S3] Th. C. Stamatatos, G. S. Papaefstathiou, L. R. MacGillivray, A. E. Escuer, R. Vicente, E. Ruiz and S. P. Perlepes, *Inorg. Chem.*, 2007, **46**, 8843.

[S4] W. T. Carnall, S. Siegel, J. R. Ferraro, B. Tani and E. Gebert, *Inorg. Chem.*, 1973, **12**, 560.

[S5] K. Nakamoto, *Infrared and Raman Spectra of Inorganic and Coordination Compounds*, 4th ed., Wiley, New York, 1986.

[S6] *Bruker APEX3* 2016; Bruker AXS Inc., Madison, Wisconsin, USA.

[S7] G. M. Sheldrick, *SADABS-2016/2* 2016, Bruker AXS Inc., Madison, Wisconsin, USA.

[S8] *Rigaku Oxford diffraction CrysAlisPro* 2015, Rigaku, Tokyo, Japan.

[S9] G. M. Sheldrick, *Acta Crystallogr., Sect. A.: Found. and Adv.*, 2015, **A71**, 3-8.

[S10] G. M. Sheldrick, *Acta Crystallogr., Sect. C: Cryst. Struct. Commun.*, 2015, **C71**, 3-8.

[S11] O. V. Dolomanov, L. J. Bourhis, R. J. Gildea, J. A. K. Howard and H. Puschmann, *J. Appl. Crystallogr.*, 2009, **42**, 339-341.